

Synchronization and extinction in a high-infectivity spatial SIRS with long-range links

Ezequiel Arceo-May and Cristian F. Moukarzel

CINVESTAV del IPN, Appl. Phys. Dept.
97310 Mérida, Yucatán, México.

E-mail: cristian.moukarzel@cinvestav.mx

Abstract. A numerical study of synchronization and extinction is done for a SIRS model with fixed infective and refractory periods, in the regime of high infectivity, on one- and two-dimensional networks for which the connectivity probability decays as $r^{-\alpha}$ with distance. In both one and two dimensions, a long-lasting synchronized state is reached when $\alpha < d$ but not when $\alpha > d$. Three dynamical stages are identified for small α , respectively: a short period of initial synchronization, followed by a long oscillatory stage of random duration, and finally a third phase of rapid increase in synchronization that invariably leads to dynamical extinction. For large α , the second stage is not synchronized, but is instead a long-lasting endemic state of incoherent activity. Dynamical extinction is in this case still preceded by a short third stage of rapidly intensifying synchronized oscillations. A simple model of noise-induced escape from a potential barrier is introduced, that explains the main characteristics of the observed three-stage dynamical structure before extinction. This model additionally provides specific predictions regarding the size-scaling of the different timescales for the observed dynamical stages, which are found to be consistent with our numerical results.

Keywords: SIRS, Synchronization, Long-Range links, Numerical Simulation, Dynamical Systems, Disease Propagation, Neuronal Dynamics.

1. Introduction

Excitable systems [1, 2] are interacting arrays of simple units possessing an active and a dormant state. These units can be activated by contact with an already active neighbor, thereafter decaying to the inactive state. This decay proceeds in a stochastic or deterministic manner, within a characteristic decay time. Once deactivated, the unit must spend a given refractory time in the inactive state before it can be activated again.

Networks of interacting excitable units have been proposed as models of brain dynamics [1, 3, 4, 5, 6, 7], disease propagation [1, 8], and more [1]. Despite their apparent simplicity, collective effects endow these systems with interesting dynamical behaviors such as the appearance of waves, complex spatiotemporal patterns [1] and spontaneous synchronization [9].

Recurrent diseases may develop into an *endemic* stable state, where active and inactive states randomly coexist, without any kind of spatiotemporal order. The stable state is a fixed point of the dynamics in the limit of large systems. For finite populations, however, stochastic fluctuations lead to disease extinction in finite time [10, 11]. This is called extinction by chance, or spontaneous extinction. A different mechanism for activity extinction occurs through extreme synchronization [12, 8], in models that display such dynamical behavior. This last case is the focus of the present work.

Understanding the factors affecting the duration, or *persistence time*, of e.g. an epidemic outbreak, is clearly a matter of the highest relevance in epidemiological modeling. Also important are synchronization effects in the case of recurrent diseases such as Influenza A H1N1 [13] and other influenza-like diseases [14, 15, 16, 17].

Synchronization is perhaps of even greater relevance in neural systems, where it is believed to play a role in cognitive processes [18]. Extreme synchronization appears, on the other hand, to be functionwise undesirable in neural systems. It is known that certain dysfunctional behaviors such as epileptic seizures [19, 20, 21] and Parkinson's disease [22], are correlated with a high level of synchronism in certain areas of the brain. In models of excitable systems, extreme synchronism (phase ordering) implies the extinction of the dynamics, since significant numbers of both active and inactive units must be simultaneously present in order for activity to be propagated in time.

The extinction of one or more among n interacting subpopulations can be mapped onto the so-called “Exit Problem” [23], in which the vector \vec{x} of densities evolves within a space Ω , until it gets trapped by an absorbing boundary $\partial\Omega$. In the presence of stochasticity, it is helpful to think of the exit problem as that of slow diffusion of particles in a deterministic flow. The scaling of average exit times $\langle t_{exit} \rangle$ will then depend on the nature of the underlying flow. Two particular cases [24, 23] are relevant for this work. *Diffusion along a flow*: occurs when the deterministic dynamics pushes the system out from Ω . The expected exit time, in general dimension, behaves as [23]

$$\langle t_{exit} \rangle \sim \ln(N). \quad (1)$$

Diffusion against a flow: occurs when the deterministic dynamics have a stable equilibrium in Ω , so that escape occurs against the deterministic forces. The expected

exit time, in dimension one, is [23]

$$\langle t_{exit} \rangle \sim N^{-1/2} \exp(QN) \quad Q > 0. \quad (2)$$

van Herwaarden & Grasman [10] and Roozen [25] reported the same relation as Eq. (2) for the SIR model with removal-renewal and the generalized Lotka-Volterra model, respectively.

In ecology studies, the above scaling relations are observed in stochastic Lotka-Volterra models [26, 27, 28] and in stochastic SIRS models [11, 12].

For each instance of the excitable dynamics, the *extinction time* is a random variable, whose distribution equals minus the time-derivative of the *survival probability* or *persistence*, $F(t)$, estimated as the fraction of active systems at time t [29]. Understanding extinction times is of practical importance e.g. in the design of epidemiological policies (See [30] and references therein).

Ki Baek [12] mention that extinction may happen *spontaneously* (by chance), or *synchronously*. For the SIRS model in small-world networks, Kuperman & Abramson [8] reported that high values of virulence usually lead to *synchronous extinctions*.

The ability of a system to spontaneously synchronize depends on the dimension and other topological properties of the network of interactions among units [31, 32]. In the case of short-range interactions, the lower critical dimension for the appearance of cooperative synchronization is $d_c = 2$ [33, 34, 35]. Chains of Kuramoto oscillators with long-range interactions decaying as $1/r^\alpha$ do synchronize, however only for $\alpha \leq 3/2$ [36].

Recent work analyzing connections between neurons [37, 38, 39, 40] suggests that, while most of them are short-ranged [41, 42], a significant number of long-distance connections also exists [43].

One common element to various types of analyses [44, 45, 46] of brain networks is the fact that their topology is that of a small-world network, either with power-law distributed link lengths [44], exponentially truncated [45], or a combination of both [46]. At the level of functional brain networks, it has been argued that their topology has elements from small-world and scale-free networks [47] Human mobility patterns [48], which are relevant for disease propagation, also show a power-law distribution of travelled distances.

A simple model of network connectivity that allows onw to consider both short- and long-range links in a controlled manner is the power-law decay network [49]. In this model, which is the one we chose to use in this work, two nodes i and j in a d -dimensional array are connected at random with probability $p_{ij} \sim 1/r_{ij}^\alpha$, where r_{ij} is their Euclidean distance, and the decay exponent α is a tunable parameter. The density of links p is an additional parameter, which must be chosen large enough to ensure macroscopic connectedness across the system. For large α , only short-range links are present, and a d -dimensional topology is obtained. When $\alpha \rightarrow 0$, on the other hand, long links are generated and an ∞ -dimensional random graph is produced. In this article, the effects of spatial dimension d and the distribution of link lengths parametrized by α are analyzed for a SIRS [50, 8, 12, 11, 51] model of excitable dynamics on these networks. The focus

of the present work is on the analysis of synchronization and the characterization of extinction times in these networks.

Our large-scale numerical simulations show that networks with $\alpha < d$ display three dynamic stages, when starting from an incoherent state of random activity. These are: 1) a short transient of rapidly increasing synchronization, followed by 2) a relatively large period of sustained moderate coherence, and finally, 3) a short burst of rapidly increasing coherence, that invariably leads to extreme synchronization and extinction. When $\alpha < d$, we argue that the extinction process can be seen as noise-mediated escape from a stable periodic orbit. For large α , on the other hand, there is no synchronized second stage, and the extinction of the dynamics can be understood as an extreme-synchronization mediated escape from a fixed point. Rationalizing the extinction problem as one of stochastic escape from an attractive periodic orbit *or* fixed point, extinction times are expected to scale in a similar way as those for escape against a flow mentioned above, i.e. as $\log(t_{1/2}N) \sim N$. Our numerical measurements are found to be consistent with this expectation. In all cases the timescale for extinction is found to grow exponentially fast with increasing system size N . Notice that, because we work in the regime of large infectivity, our results apply to the limit of weak noise. The large-noise case, in which spontaneous extinction is predominant, may have different scaling properties [11].

The rest of this article is organized as follows: Section 2 describes the networks and dynamical model we use, discussing details of implementation, numerical simulation, and measurement procedures.

Section 3 presents our numerical results, as follows: Sections 3.1 and 3.2 describe the observation and characterization of dynamical stages leading to extinction.

Section 3.3 introduces our model for escape from a periodic orbit. Its predictions are discussed and compared with numerical results in Sections 3.4, 3.5, and 3.6. In Section 3.7 the α -dependence of the involved timescales is discussed, analyzing evidence for a dynamical phase transition that is seen in one dimension but not in two. Finally, Section 4 presents a general discussion of our results.

2. Model and Methods

2.1. SIRS model

SIRS is a simple model of excitable systems that is able to reproduce some important characteristics of neuronal networks and recurrent diseases, such as oscillations and spatial waves [50, 51]. SIRS dynamics is defined, at each timestep, by the following three transition rules:

- $S \rightarrow I$: a susceptible individual having k infectious neighbors becomes infected with probability $p = 1 - (1 - p_0)^k$, where $p_0 \in [0, 1]$ is the *link infectivity*.
- $I \rightarrow R$: an infected individual becomes refractory exactly τ_i timesteps after being infected.
- $R \rightarrow S$: a refractory node becomes susceptible after τ_r time steps.

Only the $S \rightarrow I$ transition is stochastic and depends on the node's environment. The other two transitions are deterministic and happen at pre-specified times after infection. Because of this, at a given simulation time, the state of node i is entirely determined [8] by the time t_i of its last infection, as follows: node i is infectious if $0 \leq t - t_i < \tau_i$, refractory if $\tau_i \leq t - t_i < \tau_A = \tau_i + \tau_r$, and susceptible if $t - t_i \geq \tau_A$. Here τ_i , τ_r and τ_A are, respectively, the *infectious*, *refractory*, and *active* periods. Since the time that a node spends in the susceptible state is a stochastic variable, SIRS behaves as a collection of *non-identical oscillators* with different frequencies.

The phase θ of an active node i is defined [8] as $\theta_i = 2\pi(t - t_i)/\tau_A$. From these, a synchronization order parameter is defined by [52, 53]

$$ze^{i\Theta} = \frac{1}{N_a} \sum_{j=1}^{N_a} e^{i\theta_j}, \quad (3)$$

where the modulus z of the phase vector is the *coherence*, Θ is the *mean phase*, and N_a the number of active (i.e. $I + R$) sites. The system is initialized by assigning a uniformly distributed infection time $t_i \in [0, \tau_A]$ to every node i , and setting $t = \tau_A$. To actually implement the SIRS dynamics, we use a procedure that significantly speeds up numerical simulation. We begin by defining a node to be *infectible* if: a) it is susceptible and it has at least one infected neighbor, or b) it is a refractory node with at least one infected neighbor that will still be infectious when the refractory node becomes susceptible. Infectible nodes constitute the *surface* where the non-deterministic part of the dynamics, i.e. the $S \rightarrow I$ transitions, takes place. Equivalently, for each infected node i , all its neighbors j with $t_i - t_j > \tau_r$ are infectible.

In our simulations, and given the starting set of infection times $\{t_i\}$, we first set up a queue containing infectible sites. Each site i in the infectible queue is considered in turn for stochastic infection. If i does not get infected, then it is resent to the end of the queue, unless all of its infected neighbors have already healed, in which case we i is just ignored. If on the other hand i does become infected, we set its infection time $t_i = t$, and send its infectible neighbors to the end of the queue, using the simple rule mentioned above to identify them. One sweep through the entire queue of infectible nodes constitutes a time-step, after which the time variable t is advanced by one unit. The simulation ends when the queue of infectible sites becomes empty. This procedure is significantly faster than visiting all nodes, since only infectible nodes must be considered. As a consequence, we obtain a speed gain of about $\times 10$.

2.2. Networks in d dimensions with power-law distribution of link lengths

We next describe how d -dimensional networks of N nodes, randomly connected via M long-range connections, are constructed in this work. We intend to build networks for which the probability that an arbitrary pair (i, j) is connected by a link behaves as $p_{i,j} \propto r_{ij}^{-\alpha}$, where r_{ij} is the Euclidean distance between nodes i and j . Here α is the *connectivity decay exponent*, or link-exponent, for short. Starting from a set of nodes in d -dimensional space, when α is zero a random graph is obtained, in which each pair

of sites is connected with equal probability $p_{ij} = 2M/(N(N-1))$. For large α , on the other hand, only short-range links are generated, and a d -dimensional network with connectivity disorder is obtained.

Among several possible numerical procedures to obtain the desired dependence of link-connectivity on Euclidean distance r , we chose, for practical reasons, the one that follows. Initially, $N = L^d$ nodes/sites are assigned to the vertices of a hyper-cubic d -dimensional lattice of linear dimension L without any links. For coding convenience, helicoidal boundary conditions are used. We next generate M links with random lengths ℓ , distributed according to

$$p(\ell) = A\ell^{-\alpha+d-1} \quad \ell_{min} \leq \ell \leq \ell_{max}, \quad (4)$$

and use each of them to connect a randomly chosen pair of sites, provided the distance between them is approximately ℓ . $\ell_{min} = 1$ and $\ell_{max} \sim L/2$ are, respectively, the lower and upper bounds for link lengths on a finite system. This produces a random network with approximately Poisson degree distribution and average degree $\langle k \rangle = 2M/N$, in which the connectivity probability decays as $r^{-\alpha}$. Notice the extra $d-1$ in Eq. (4), which accounts for the number of sites at a distance ℓ from a given one in d dimensions. In this work, networks embedded in $d = 1$ and $d = 2$ dimensions were generated, using the procedure sketched above.

Because of the sparsity and randomness of our networks, a large number of connected components can in general coexist. However, a large enough $M = 2N$ is always used, $M/N = \langle k \rangle / 2 = 2$, so that the largest connected component typically contains a large fraction of the system. In other words, we work well above the percolation critical density of links, located at approximately $\langle k \rangle_c = 1$ [54].

For each value of d , α and L , we performed 10^3 repetitions of the dynamics until extinction on a newly generated network. Simulation of systems with several values of α for moderate size as $N = 40 \times 40$ up to extinction required weeks of cpu time in total.

Because of the numerical difficulties associated with long extinction times on large static networks, we devised an annealing procedure that, we found, speeds up the dynamics of the system. We take a fixed small *annealing probability* p_a and, at each time step, reallocate a total of $p_a \times M$ links (both edge-ends). Since link-lengths are unchanged, this procedure produces a slightly different network with the same length distribution as the original one. We found that the synchronization and extinction process happens faster on annealed networks than on static networks. Static properties measured over annealed networks with small values of p_a , however, were found to present the same quantitative behavior as on static networks without annealing. The dynamical behavior is also similar on annealed networks, only on shorter timescales.

2.3. Measurement procedure

For each repetition of the experiment, which involves a newly generated network, we determine the *extinction time* t_{ext} , i.e. the number of timesteps at which the queue

of infectible sites becomes empty. We find that both the average and dispersion of this random variable increase exponentially fast when L increases. We are also interested in estimating the distribution of extinction times $P(t_{ext})$. The cumulative distribution of extinction times is related to the survival probability or *persistence*, $F(t) = \int_t^\infty P(t_{ext}) dt_{ext}$, which we estimate as the fraction of still active systems at time t [29]. The persistence *half-time* $t_{1/2}$ is defined by the condition $F(t_{1/2}) = \frac{1}{2}$, i.e. the time at which roughly one half of all starting configurations have become extinct.

For most observables of interest we take measurements, and average their results over repetitions of the experiment, at geometrically increasing time intervals $t_k \sim a^k$. Additionally, a second measurement protocol was implemented in order to study the final stages of the dynamic. To this end, a circular array of “diameter” 10^4 is kept, that saves results from the last 10^4 timesteps. We average these “final stage” data after each simulation ends, in such a way that measurements at extinction coincide for different repetitions of the experiment. This allows us to obtain averages that are representative of typical behavior on approach to extinction. We denote the time measured backwards from extinction, $t_{te} = t_{ext} - t$, as *time-to-extinction*.

Averages were taken in all cases over 1000 networks, with one random starting configuration per network, for each set of parameters. Link infectivity p_0 was fixed to 0.75, a relatively large value, which makes spontaneous (i.e. not mediated by extreme synchronization) extinctions unlikely [8]. The infectible period was set to $\tau_i = 4$, and the refractory period to $\tau_r = 8$.

3. Simulation results

3.1. Synchronization and its α -dependence

Let us begin by discussing the basic observable features of the synchronization process in these networks. As mentioned previously, we have chosen a value for the link infection probability that is large enough to ensure synchronization-induced extinctions. Therefore, we expect that spontaneous extinctions will not be relevant.

Figs. 1 and 2 show the coherence z , the phase variance σ , and the persistence F , resulting from averages over 10^3 realizations in $d = 1$ and 2 dimensions, for chosen values of the link exponent α , on static ($p_a = 0$) networks. Networks with link-annealing ($p_a > 0$) produce similar results, but on shorter timescales. At the beginning of a simulation, z is low and σ is large, because node phases are initially distributed at random over the active period. When $\alpha \leq d$, two dynamical stages are clearly distinguishable: The first one is the stage of *Initial Synchronization*. During this stage, the coherence z increases and the phase dispersion σ decreases, until both stabilize after approximately 10^2 to 10^3 steps. No extinctions occur during this initial organization period, i.e. the persistence $F(t)$ stays exactly at one. Next comes the stage of *Sustained coherence*. During this second stage, the average coherence z shows a constant value, and so does σ . Extinctions start to occur in this stage, as evidenced by a decreasing value of the persistence $F(t)$. Notice,

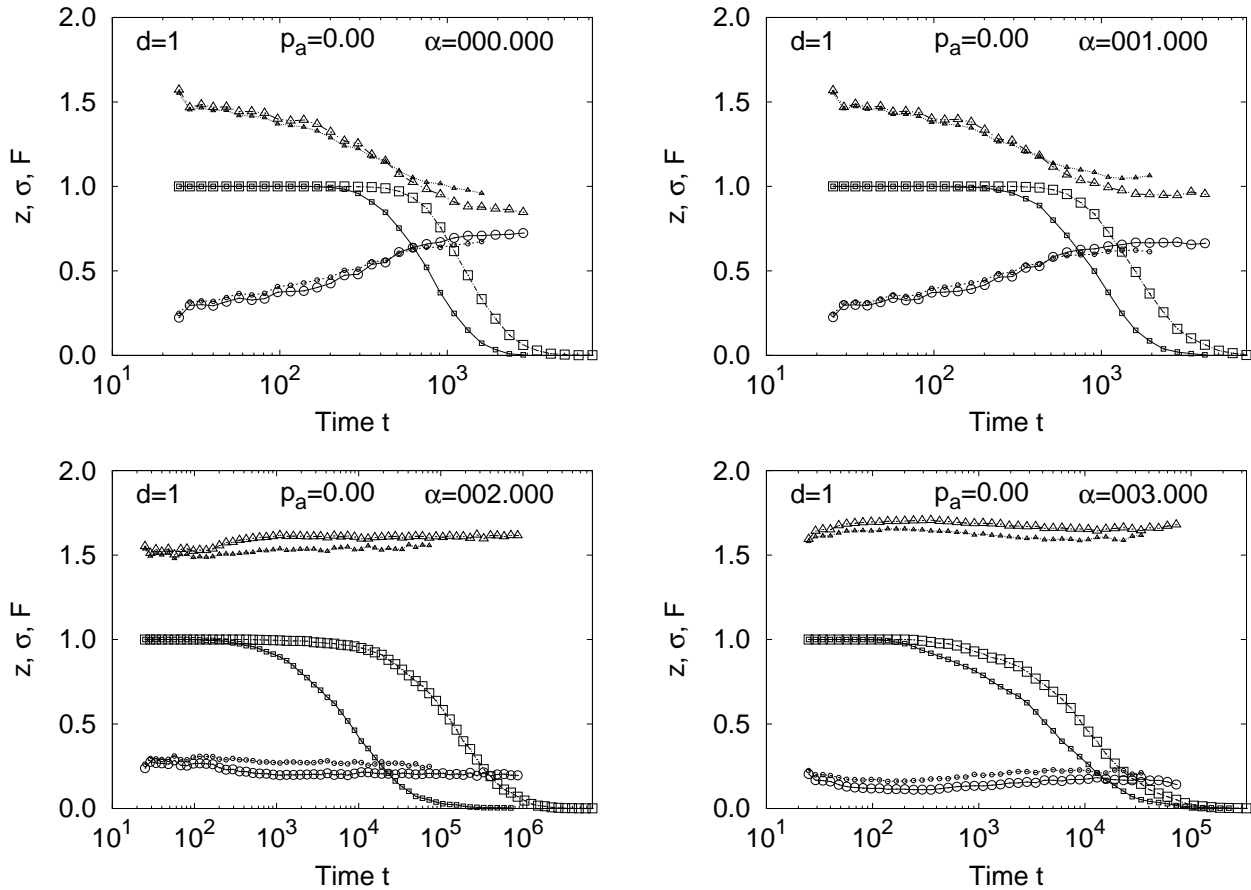


Figure 1. Persistence (squares), Coherence z (circles) and phase dispersion σ (upwards triangles) vs time in one-dimensional networks with $L = 200$ (small symbols) and $L = 400$ (large symbols) for several values of the link power-law decay exponent α .

however, that for $\alpha > d$, synchronization during stage two diminishes with increasing α . In this case, after a short-lived synchronization period, z decreases and σ increases again in time (Figs. 1 and 2). Synchronization, as measured by z , becomes weaker for larger systems (Fig. 3), suggesting that no synchronized stage exists in the thermodynamic limit for large α . Networks with large α are topologically d -dimensional because all links are short-ranged. In order to further explore the α -dependence of synchronizability in these networks, we measured $z_{1/2}$, the average coherence at the median time $t_{1/2}$ for extinction, (when half the samples still survive). These results are displayed in Fig. 3. They suggest that synchronization only happens, in the thermodynamic limit, for $\alpha \leq d$, in both one and two dimensions, although more extensive work would be needed in order to determine the critical value of α precisely. Furthermore, the value of the annealing parameter p_a does not seem to modify these static results significantly, although annealing does speed up the dynamics of the synchronization process (see later).

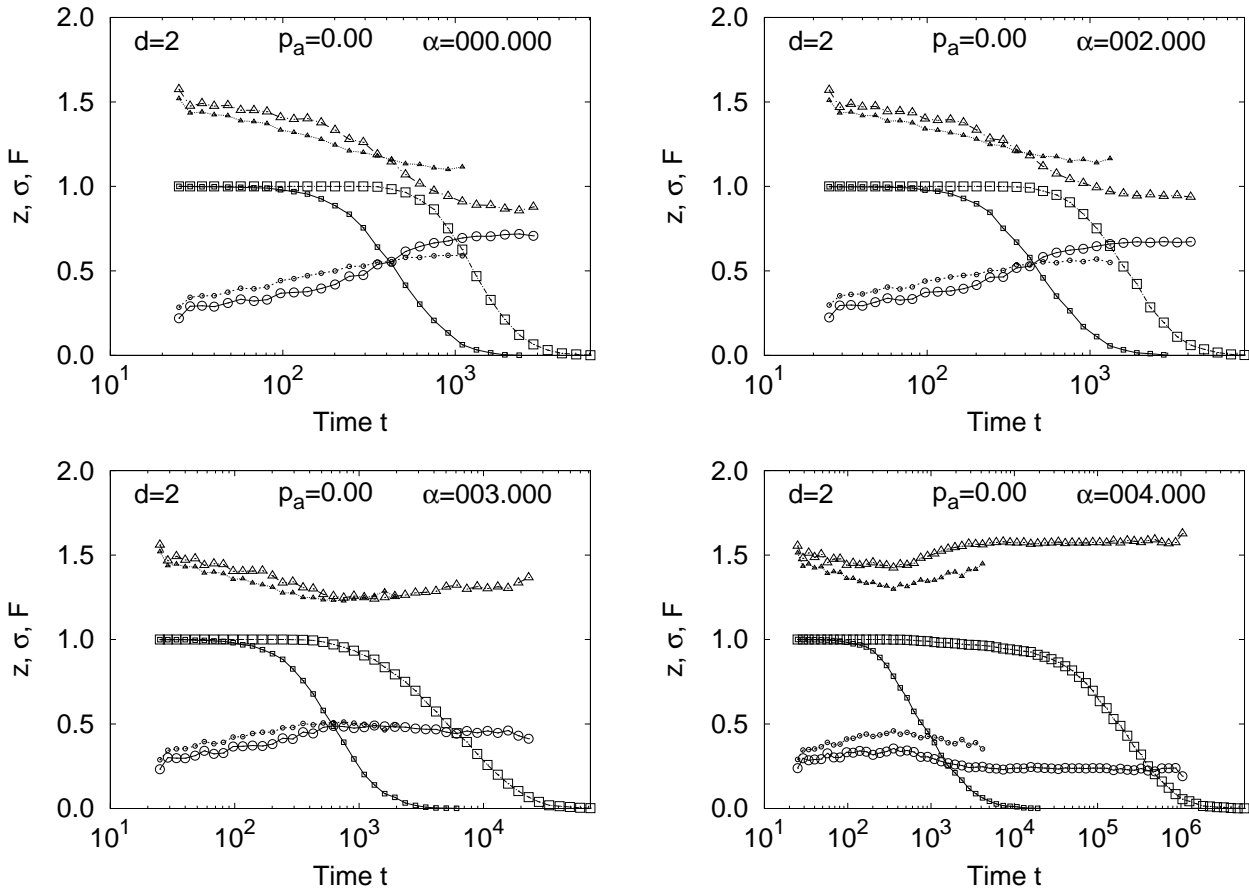


Figure 2. Persistence (squares), Coherence z (circles) and phase dispersion σ (upwards triangles) vs time in two-dimensional networks with $L = 10$ (small symbols) and $L = 20$ (large symbols) for several values of the link power-law decay exponent α .

3.2. Late-stage extreme synchronization

The data displayed in Figs. 1 and 2 would seem to suggest that extinctions happen while the system is in a state of partial synchronization (in stage two). Actually, however, this is not true. Extinction events are in fact invariably preceded by a short burst of extreme synchronization. In this last stage, which inevitably leads to extinction, the coherence z increases, and the phase dispersion σ^2 decreases rather abruptly, within roughly 10^3 timesteps (See Figs. 4 and 5). The above mentioned late-stage increases in coherence are not seen in Figs. 1 and 2, because the distribution of extinction times is so broad that these short-lived bursts of extreme synchronization do not contribute to the sample-averages.

In order to clearly reveal the true dynamical behavior of the system immediately before extinction, we recorded, for each simulation, results from the last 10^4 timesteps (using a circular array). These data were subsequently averaged in such a way that extinction times coincide for all simulations, and taking averages at equal values of the *time-to-extinction* t_{te} . These measurements in “reverse time” are displayed in Figs. 4 and 5 versus t_{te} . They show that the coherence z increases steeply, and the phase

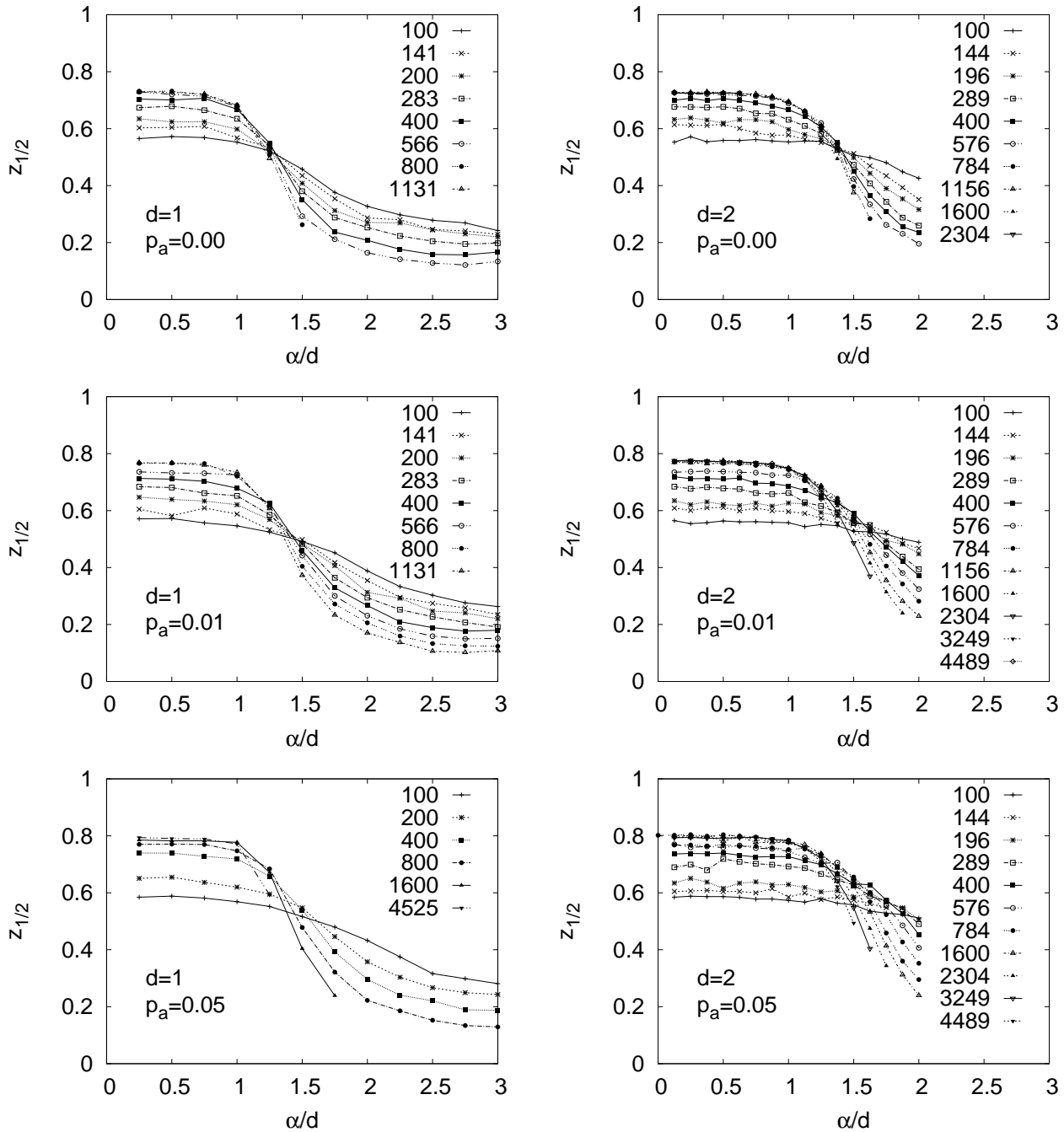


Figure 3. Coherence z , averaged over 1000 networks, taken at halftime $t_{1/2}$ for extinction, vs link-length exponent α , for several system sizes N (labels of symbols in each plot) and for different amounts of link annealing p_a . Plots on the left are for one-dimensional networks, those on the right for two-dimensional ones. These results suggest that a synchronized second stage exists only for $\alpha < d$ in both one and two dimensions. Symbol labels indicate the number N of sites in the system.

dispersion σ decreases, right before extinction. Therefore, at a random time and while on stage two, the system starts to synchronize even more, and does so rather rapidly. Approximately 10^2 to 10^3 steps later, extinction of the dynamics invariably happens.

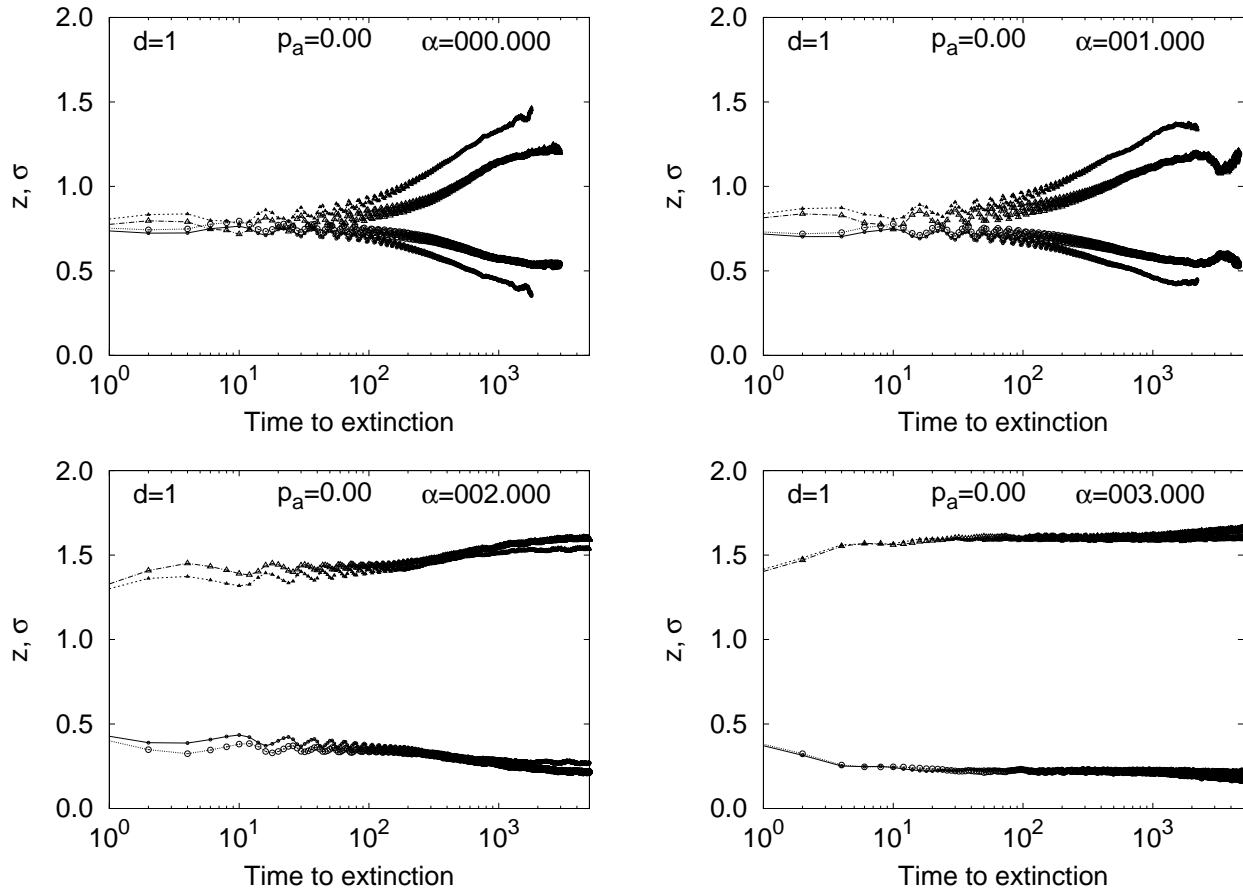


Figure 4. Coherence z (circles) and phase dispersion σ (upwards triangles) vs time-to-extinction in one-dimensional networks with $L = 200$ (small symbols) and $L = 400$ (large symbols) for several values of the link power-law decay exponent α .

Therefore, some random event (see later for a discussion) seems to occur during stage two, after which the system inevitably undergoes extreme synchronization and becomes extinct. Notice that different realizations of the experiment are synchronized *with each other*, when considered at equal values of t_{te} , as evidenced by the oscillations seen in Figs. 4 and 5. This implies that all extinctions occur at the same point during the oscillatory phase of the system, and also that the final steps of the dynamics are similar, and occur in phase with each other, for all network realizations. We can therefore conclude that there is in fact a third dynamical stage, with an approximate duration of $10^2 - 10^3$ timesteps for most of the cases analyzed here, during which the system undergoes extreme synchronization, and which inevitably leads to the extinction of the dynamics.

We furthermore notice that stages one and three are relatively short, while stage two is by far the longest (for large systems), with an average duration that increases very fast with system size. The time that a system spends in stage two is a stochastic variable with a distribution that broadens with increasing system size. (see Section 3.4). The permanence time of the system in stages one and three, on the other hand, is almost

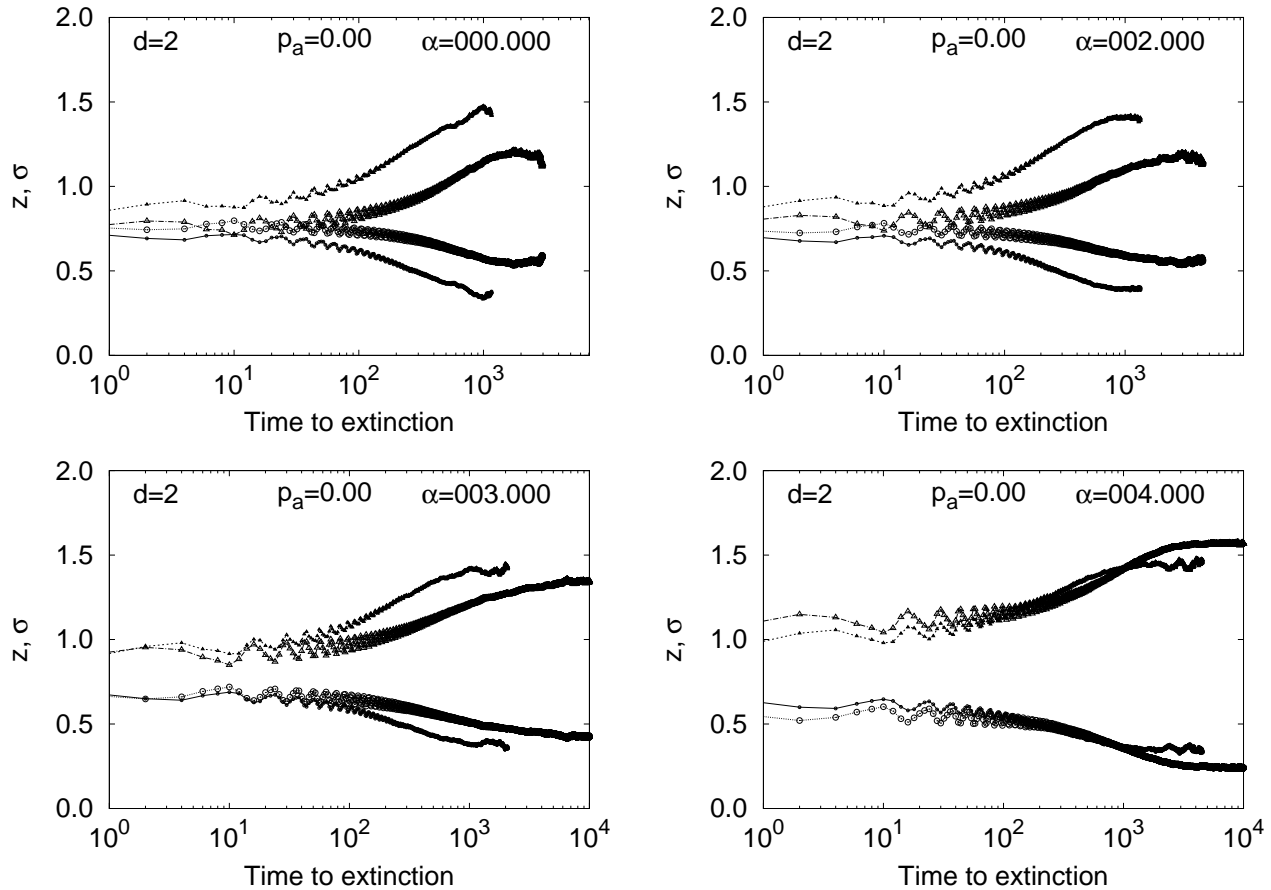


Figure 5. Coherence z (circles) and phase dispersion σ (upwards triangles) vs time-to-extinction in two-dimensional networks with $L = 10$ (small symbols) and $L = 20$ (large symbols) for several values of the link power-law decay exponent α .

deterministic. Let us mention that the initial “resilience time” τ_0 during which the persistence $F(t)$ stays at one, corresponds to the added durations of stages one and three, which is the minimum amount of time after which an extinction can happen. In this work we will not discuss how to separately measure the length of stages one and three.

Fig. 6 shows the last 400 steps of the location of \vec{T} in phase-space on approach to extinction, averaged for equal time-to-extinction. Far from extinction, there are small-amplitude oscillations in densities, whenever stage two is synchronized (for small α , left), or none at all when stage two is a fixed point (for large α , right). The amplitude of oscillations increases shortly before extinction (black square), which occurs on the RS line of the outer boundary, i.e. when no more infected (I) sites remain.

Notice that the amplitude of oscillations, early before extinction, may be underrepresented in these plots. Different realizations of the experiment, even if internally synchronized, are not in synchrony *with each other* too long before extinction. This is due to slight differences in oscillation periods, which in turn produce phase differences that are zero near extinction (because we make extinction points coincident).

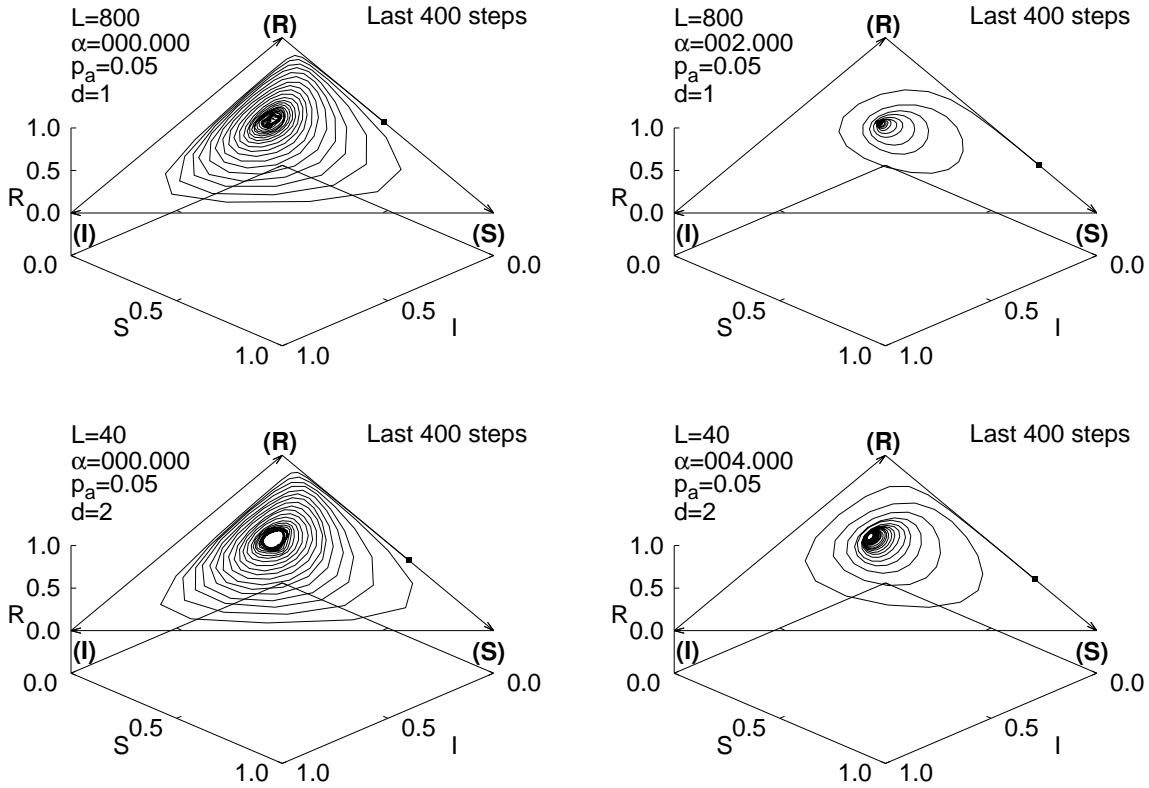


Figure 6. Phase-space location of the triad $\vec{T} = (R, S, I)$, averaged over 1000 networks at equal time-to-extinction, in $d = 1$ (top) with $L = 800$, and $d = 2$ (bottom) with $L = 40$. Plots on the left are for $\alpha/d = 0$, those on the right for $\alpha/d = 2$. In all cases the annealing rate per link is $p_a = 0.05$, and only the last 400 steps are shown.

when averaging), but are large and destroy inter-sample coherence at early times. However, consideration of Figs. 4 and 5, where the coherence z is first measured for each sample and only later averaged over samples, allows one to be certain that stage two has nonzero coherence for small α .

3.3. Extinction as escape over a potential barrier

The basic features of the extinction process, discussed in the previous Section, are as follows. As Figs. 1 and 2 show, the persistence $F(t)$ stays at exactly one during a “resilience time” τ_0 . There are no extinctions at all during this period. Once the system has synchronized partially, on stage two, a randomly occurring event triggers a sudden increase in synchronization (the system enters stage three) and extinction happens inevitably soon thereafter.

These observations can be rationalized by means of an approximate treatment, as follows. Consider the triad $\vec{T} = (R, S, I)$ formed by the fractions of Refractory, Susceptible, and Infected sites in the system. Since $R + S + I = 1$, this triad is constrained to a plane. Non-negativity of fractions further constrains \vec{T} to the interior

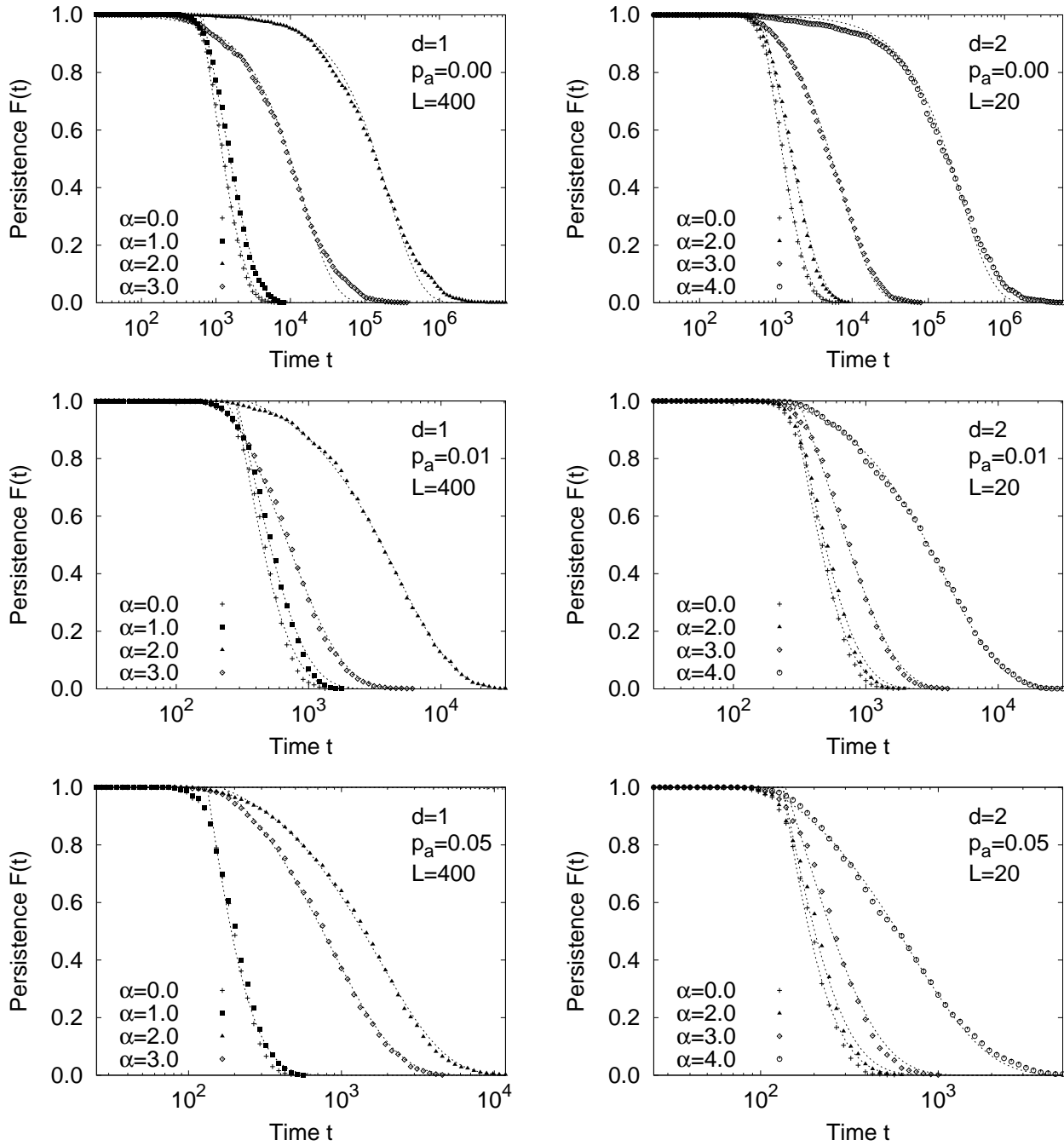


Figure 7. Persistence $F(t)$ estimated as the fraction of samples still active at time t , for the SIRS model discussed in this work in one (left) and two (right) dimensions, for several values of the link-exponent α (symbol labels). In all cases, the number of sites in the system is $N = 400$. After a “resilient” period τ_0 , during which no extinctions occur and $F(t)$ stays at one, $F(t)$ starts to decay and does so approximately exponentially in time. Increasing the rate p_a of link-annealing only shortens the involved timescales, without significantly modifying the above described dynamical behavior. Dashed lines are exponential fits using (9), from which our estimates of τ_0 and τ_2 are obtained.

of a triangle Ω within this plane (See Fig. 6). A state of persistent asynchronous activity

(the *endemic* state of an infection) is described, in this representation, by a static point near the center of the available domain. A synchronized system, on the other hand, corresponds to a point that evolves around a closed orbit. A trajectory that approaches the external boundary $\partial\Omega$ of the available region Ω takes the system close to dynamical extinction, as can be seen by considering the time-evolution of a point on the RS line in Fig. 6). In the long run, all trajectories end up in the absorbing state $S = 1$.

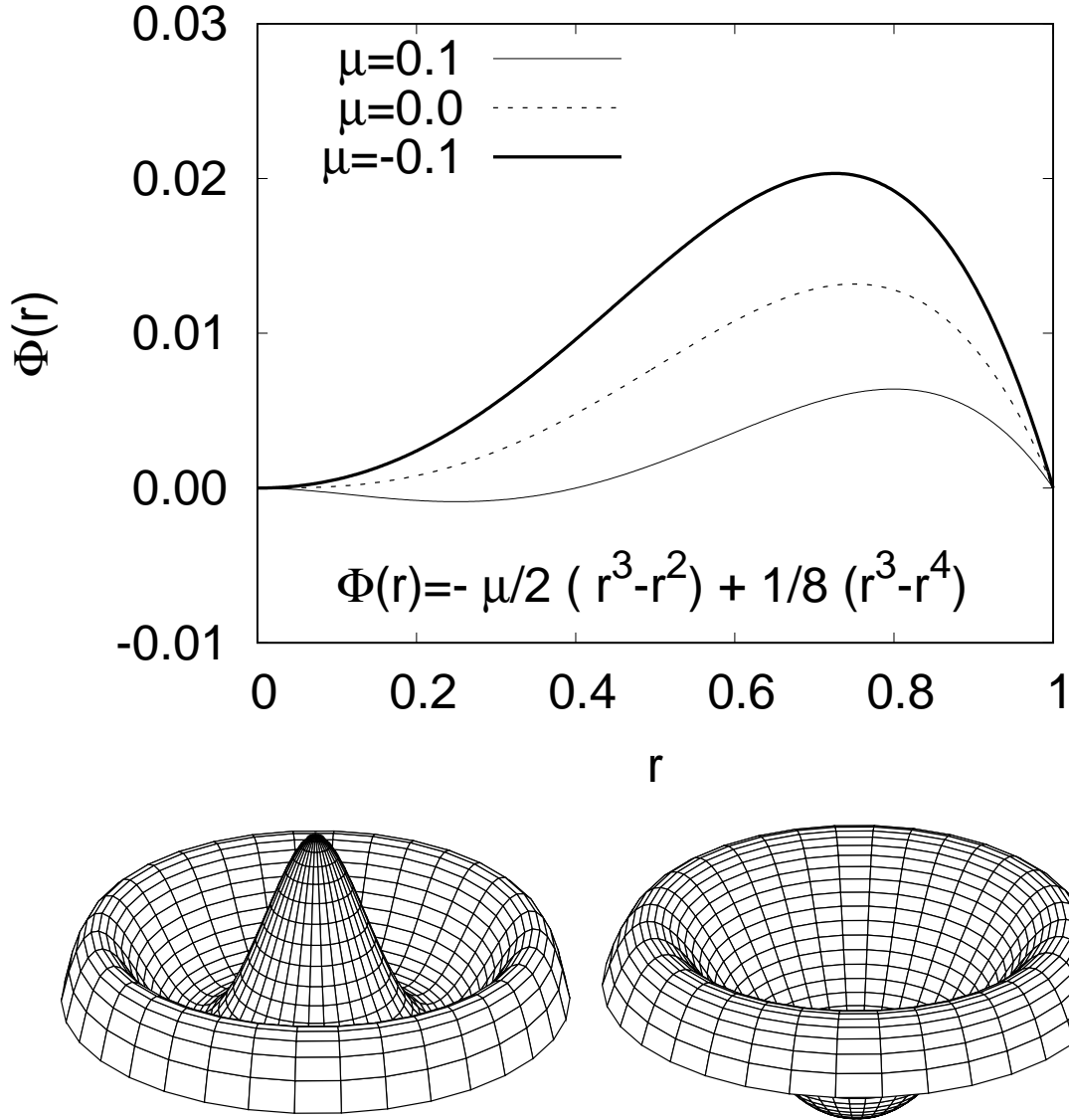


Figure 8. Radial dependence (top) of the potential surface $\Phi(r, \theta)$ (bottom) associated with the observed dynamics, both for $\alpha < d$ (top, thin line, and bottom, left) in which case there is a stable periodic orbit, and for $\alpha > d$ (top, thick line, and bottom, right), when the endemic state at $r = 0$ is stable. Notice that in both cases there is an unstable orbit (at the top of the potential barrier) engulfing the stable attractor, and beyond which the dynamics gets absorbed at the outer boundary. The case $\alpha = d$ or $\mu = 0$ (top, dashed line) may correspond to a supercritical Hopf bifurcation, taking place inside an unstable orbit.

For the sake of simplicity, assume that periodic orbits, and the external boundary $\partial\Omega$, are circular in shape, and that the endemic equilibrium state, if there is any, is located at $r = 0$, which is also the random initial state. Next, and for the sake of tractability, let us further assume that the *noiseless* dynamics of $\vec{\mathcal{T}}$ can be written, in polar coordinates, as

$$\begin{aligned}\dot{r} &= -\frac{\partial\Phi(r)}{\partial r} \\ \dot{\theta} &= \omega.\end{aligned}\tag{5}$$

Actually, the last assumption, i.e. that $\vec{\mathcal{T}}$ is a *function of state*, is a rather strong one in this context. In fact, for the SIRS model under consideration, the knowledge of $\vec{\mathcal{T}}$ is clearly not enough to calculate $\dot{\vec{\mathcal{T}}}$, because one also needs to know the time at which each site last became infected. A rigorous treatment of the mean-field dynamics for large systems [51] requires the knowledge of the entire distribution of times since last infection. The time since last infection of course determines the present state of a node, but it also provides more information. That extra information is needed in order to calculate the noiseless dynamics. However, and for the sake of mathematical tractability, we will relax that requirement, and pretend that the sole knowledge of the density of nodes in each state, i.e. knowledge of $\vec{\mathcal{T}}$, suffices to calculate the dynamics, and that the resulting equations are given by (5) for some potential $\Phi(r)$.

Furthermore, on a frame that rotates with angular velocity ω we would have

$$\begin{aligned}\dot{r} &= -\frac{\partial\Phi(r)}{\partial r} \\ \dot{\theta} &= 0,\end{aligned}\tag{6}$$

which is readily written as $\dot{\vec{\mathbf{x}}} = -\nabla\Phi(\vec{\mathbf{x}})$, where Φ is a rotationally invariant potential. In the presence of noise, the dynamical equations in the rotating frame read

$$\dot{\vec{x}} = -\nabla\Phi + \vec{\xi},\tag{7}$$

where $\vec{\xi}$ is a noise vector. Its angular component only produces phase diffusion, while its radial component is responsible for the eventual escape of the system from any existing stable attractors of the noiseless dynamics. For the purpose of representing the dynamical phenomenology observed in our simulations, we will be discussing the particular case of

$$\Phi(r, \theta) = -\mu/2(r^3 - r^2) + 1/8(r^3 - r^4),\tag{8}$$

the properties of which are illustrated in Fig. 8. For small $\mu > 0$, the endemic state at $r = 0$ is unstable, and there is a stable orbit located at $r^s(\mu)$, between $r = 0$ and the outer unstable orbit. This stable orbit attracts the noiseless dynamics. As $\mu \rightarrow 0^+$, the stable orbit radius $r^s(\mu)$ shrinks continuously to zero, until this orbit coalesces with the unstable state at $r = 0$ when $\mu = 0$. For small $\mu < 0$, the endemic state at $r = 0$ becomes a stable attractor, while the external unstable orbit modifies its radius only slightly. In the language of Dynamical Systems [55], this transformation corresponds to a *Supercritical Hopf bifurcation*. In this particular case, one occurring inside an unstable

orbit. This simple potential reproduces the observed dynamical stages if one further assumes that $\mu \propto (d - \alpha)$. Consequently, for $\alpha < d$ one has μ positive and therefore a stable periodic orbit surrounded by an unstable one. For $\alpha > d$, on the other hand, μ is negative and only the endemic state is stable, and it is still surrounded by an unstable orbit.

Let us now analyze the typical dynamical behavior of this system in the presence of noise. The radial coordinate r is proportional to the coherence and measures synchronization. The starting point is a random mixture of R, S and I , therefore non-synchronized and located at $r = 0$ within our simplified picture. For $\alpha < d$, the potential Φ has a local maximum at $r = 0$ (thin line, corresponding to $\mu = 0.1$ in Fig. 8 top, and bottom left surface in that figure). This state is unstable, so the system slides downwards towards the stable orbit, in which constitutes stage one of the dynamics. The period of variable duration spent at or near the stable orbit is stage two. Eventually, a fluctuation pushes the system over the external potential barrier, after which it enters stage three. During stage three, synchronization increases rapidly until the system gets absorbed at the external circular boundary.

When $\alpha > d$, the state $r = 0$ is a minimum of Φ (thick line, corresponding to $\mu = -0.1$ in Fig. 8 top, and bottom right surface in that figure), and therefore locally stable. The system does not synchronize initially, but fluctuates around the endemic state ($r = 0$ in this case) until noise allows it to escape over the unstable orbit, entering stage three to extinction. Significant synchronization only occurs during stage three. Our system would thus undergo a supercritical Hopf bifurcation [55] at $\alpha = d$. For the particular SIRS model studied here, this supercritical bifurcation is located inside a passive unstable orbit, which gives rise to stage three of the dynamics (rapid synchronization leading to extinction).

In addition to just providing a simple graphical illustration of the origin of the observed three dynamical stages, this model makes very specific scaling predictions that can be tested against numerical results. In the presence of weak noise, and for $\alpha < d$, one expects to see three distinct dynamical stages, when starting from a state of random activity near the central peak of the potential: An initial, downward moving stage of synchronization lasting for τ_1 steps, followed by a synchronized stage of stochastic duration t_2 , and finally a third stage of increasing synchronization that leads to extinction after τ_3 steps. The durations τ_1 and τ_3 of stages one and three are expected to be well defined (not stochastic) if the amount of noise is small, because during these stages the dominant forces are the deterministic ones. But the permanence time t_2 of the system stage two, being related to a process of noise-induced escape against deterministic forces, should be strongly stochastic.

The distribution of t_2 and the scaling with N of the involved timescales is discussed in the following Sections, and compared with predictions stemming from the noise-activated-escape picture discussed above.

3.4. Exponential distribution of permanence times in stage two

Using concepts from the theory of First-Passage processes [56], one can conclude that, due to the finite character of the segment in which the radial variable executes its escape process, the distribution of escape times from the minimum of the potential must be asymptotically exponential, with a dominant timescale that we denote by τ_2 .

Before an extinction can take place, the system must at least traverse stages one and three, which have a combined duration, of $\tau_0 = \tau_1 + \tau_3$ timesteps. Therefore, the persistence $F(t)$ has to be rigorously equal to one during a “resilience period” of τ_0 timesteps, and it has to decay exponentially for long times. To first approximation, one can expect a functional form like

$$F(t) = \theta(\tau_0 - t) + \theta(t - \tau_0)e^{-(t-\tau_0)/\tau_2}, \quad (9)$$

where θ is the Heavyside step function, and $\tau_0 = \tau_1 + \tau_3$ is the added length of stages one and three. The permanence time t_2 of the system in stage two is a stochastic variable with an exponential distribution characterized by a unique parameter τ_2 .

We estimate τ_0 and τ_2 by fitting (9) to our data for the persistence $F(t)$, in 1d and 2d, for $p_a = 0.00, 0.01, 0.05$ and for several system sizes and values of α . A subset of these data are shown in Fig. 7 together with their corresponding fits. The resulting estimated values of τ_0 and τ_2 are presented in Figs. 9 and 10.

3.5. Scaling of resilience time τ_0 with system size N

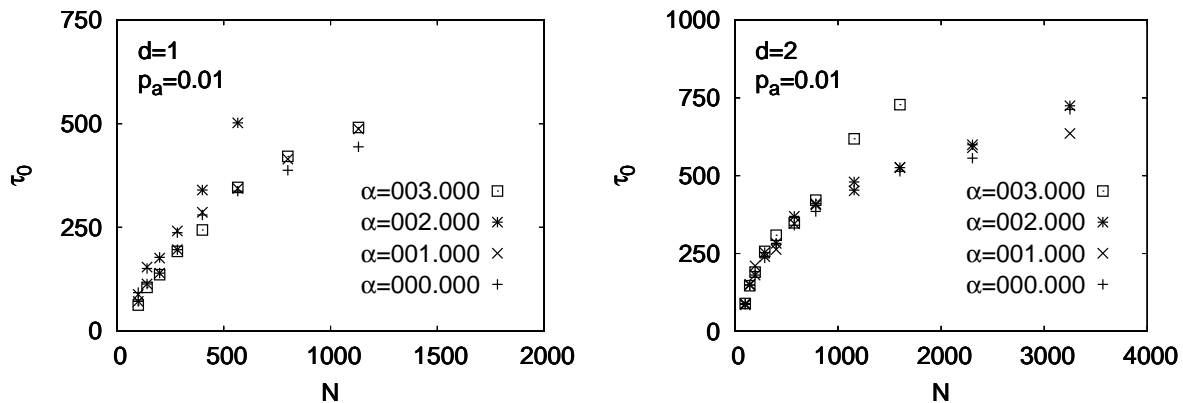


Figure 9. Scaling with system size N , of the “resilience time” τ_0 during which the persistence $F(t)$ stays at one, in one (left) and two (right) dimensions, for some values of the link-length exponent α . Theoretical considerations discussed in the text make one expect a logarithmic scaling of the form $\tau_0 \sim \log(N)$, which is consistent with the behavior seen in these plots.

Results for the estimated values of the resilience time τ_0 , obtained from fits of (9) to our data, are presented in Fig. 9. As seen in these figures, our results are consistent with a logarithmic growth of the type $\tau_0 \sim \log N$.

According to the mental model depicted in Fig. 8, the resilience time τ_0 is the time it takes for the system to slide downwards from the starting state onto the stable orbit (in case one exists), plus the time from the ridge to the outer boundary, where extinction takes place. Both are diffusive motions along a flow, and therefore a logarithmic scaling with N is expected [23]. This expectation is well verified by the data displayed in Fig. 9.

3.6. Scaling of escape timescale τ_2 with system size N

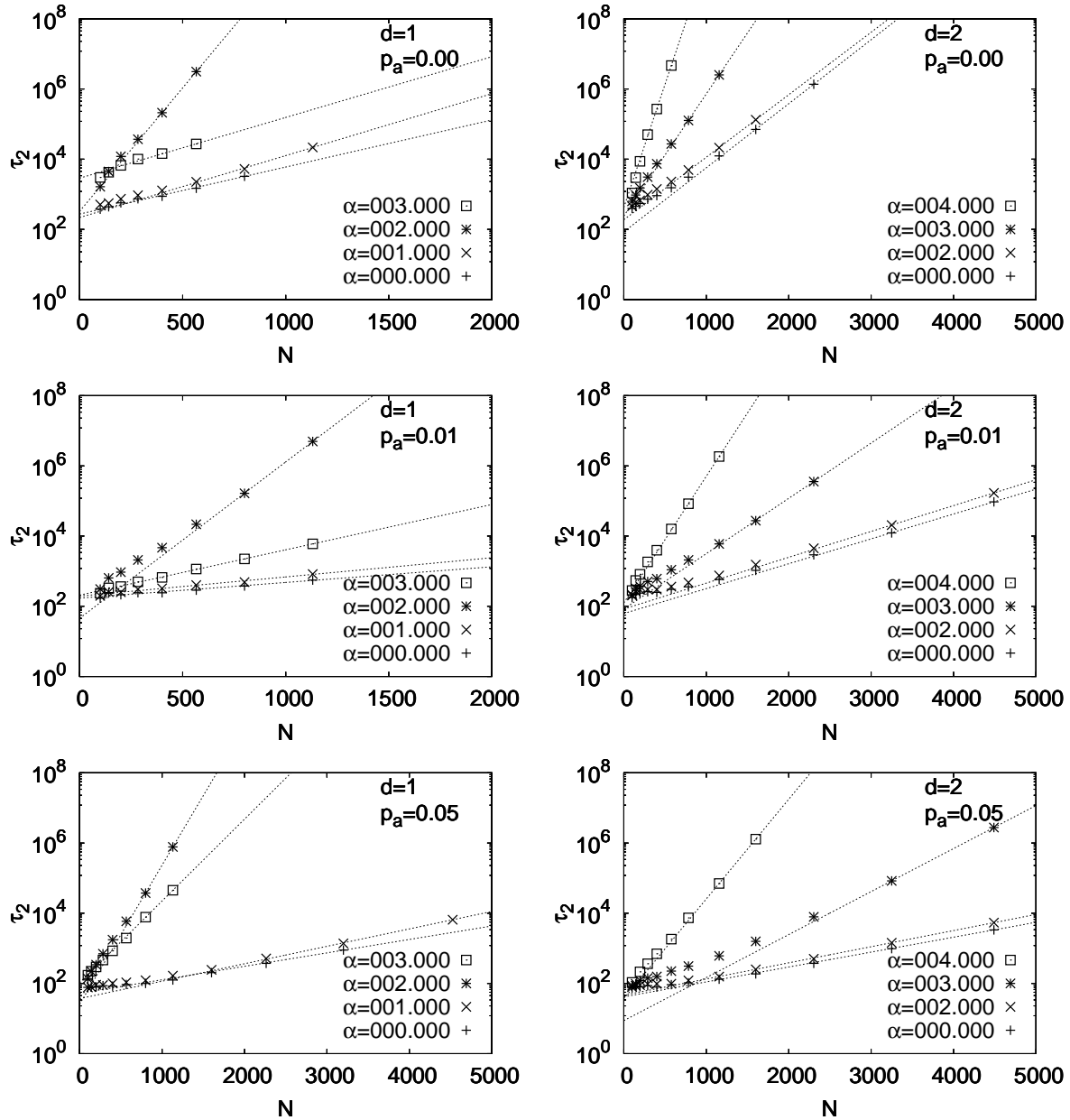


Figure 10. Timescale τ_2 for permanence in stage two (See (9)) versus system size N in one (left) and two (right) dimensions, for three values of the network-annealing parameter p_a , and for several values of the link-length parameter α . An asymptotically exponential growth of τ_2 with N is seen in these plots.

The escape process from the stable orbit to the ridge is, in the scenario of Section 3.3 and Fig. 8, a noise-induced escape against a flow, that is, escape over a potential barrier. In this case, $\log(\tau_2 N^{1/2})$ is expected to scale linearly with system size N [10]. Asymptotically, one would therefore expect $\tau_2 \sim e^{\kappa_2 N}$ to hold.

Our results for the estimated values of τ_2 , presented in Fig. 10, are in fact consistent with the expectation that, for large N , the logarithm of the dominant timescale τ_2 for permanence in stage two increases linearly with N , thus confirming the abovementioned expectations.

3.7. Speed of growth κ_2 of τ_2 with size N

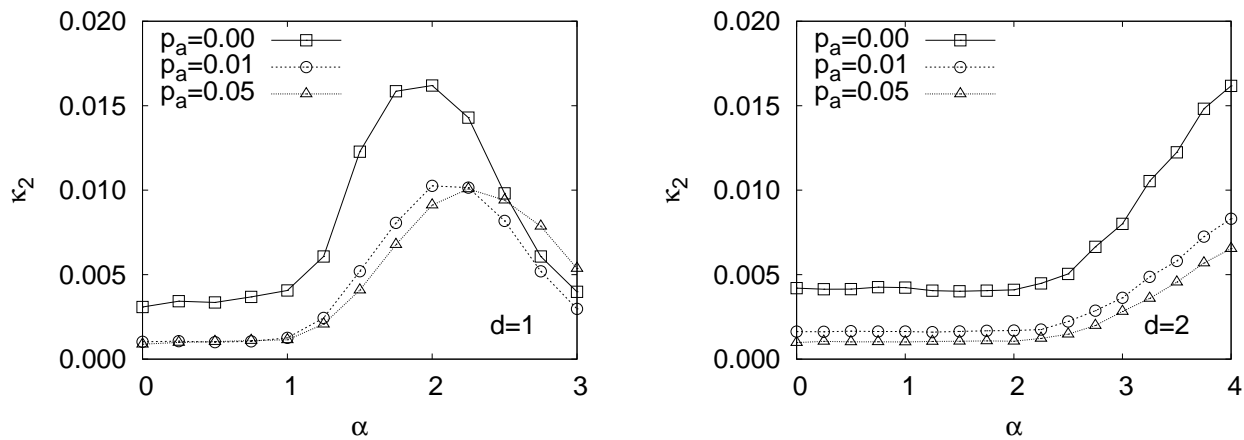


Figure 11. Logarithmic speed of growth κ_2 vs size N of the timescale τ_2 for escape from stage two of the dynamics. In one dimension (left) there is a maximum in κ_2 near $\alpha = 2d = 2$, which is not seen in two-dimensions (right).

As discussed in previous sections, our results show that $\tau_2 \sim e^{\kappa_2 N}$ asymptotically. We determine $\kappa_2(d, \alpha)$ as the slope of the asymptotic linear fits shown in Fig. 10. Our results are presented in Fig. 11 in one and two dimensions, for three values of the annealing probability $p_a = 0, 0.01$ and 0.05 used in this work. In one dimension, κ_2 is found to have a maximum, for any amount of annealing, near $\alpha \approx 2$. This hints at some kind of dynamical phase transition, since escape times appear to diverge much faster with system size in the neighborhood of $\alpha = 2$. This maximum is apparently not observed in two dimensions, where we have explored a few instances with large values of α (up to $\alpha = 8$), without seeing a decrease in escape times as the one observed in one dimension. We cannot discard, however, that a similar nonmonotonic behavior of $\kappa_2(\alpha)$ occurs in two dimensions as well, for larger systems and/or values of α , although this does not seem probable. Furthermore, more work would be needed in order to clarify the precise meaning of the maximum in κ_2 that is observed in one dimension near $\alpha = 2$.

4. Conclusions and Discussion

We analyzed the process leading to dynamical extinction in a high-infectivity SIRS model with fixed infectious ($\tau_i = 4$) and refractory ($\tau_r = 8$) periods, on long-range connected networks of N sites in one and two dimensions. The direct-link connectivity probability p_{ij} for an arbitrary pair of sites i and j at a distance r_{ij} from each other, decays as $1/r_{ij}^\alpha$. There are two links per site, which ensures that most sites belong to the largest connected component.

We focused on the synchronization and extinction properties of these excitable systems, and their dependence on N and α . Starting from a random mixture of Refractory, Infected, and Susceptible sites, when $\alpha < d$ the system first undergoes partial synchronization and then, after a varying amount t_2 of time, the coherence increases even further and the dynamics becomes extinct (the number of infected sites becomes zero). The link infectivity is $p_0 = 0.75$, large enough to ensure that spontaneous extinction of the dynamics, not mediated by synchronization, is not relevant [8].

In addition to static networks with a fixed set of links, we also analyzed annealed ones. For these, at each timestep, each link is replaced by an equally distributed one with probability p_a . In this work we used three values of annealing: $p_a = 0.00, 0.01, 0.05$. We find that annealing only shortens the dynamical timescales involved in the synchronization and extinction processes, while keeping all static results quantitatively unmodified.

In Section 3 we argue that for $\alpha < d$, the dynamical extinction process can be decomposed into three dynamical stages that are described as follows: First a short period of rapid synchronization starting from a random state. This first stage lasts for approximately 10^3 timesteps for the sizes studied here (See Figs. 1 and 2). Once the system is dynamically organized and displays sustained oscillations, it stays in this “partially synchronized” second stage for a (large) random amount of time. At a random time while in stage two, a sudden increase in synchronization happens, spanning approximately 10^3 steps (See Figs. 4 and 5), which we call Stage three, and which inevitably leads to the extinction of the dynamics. When $\alpha > 2$, on the other hand, stage one does not exist, stage two is a non-synchronized endemic state lasting for a random amount of time, after which stage three happens as described above.

In Section 3.3 we showed that all three stages of the dynamics have an interpretation in terms of the potential depicted in Fig. 8, in the presence of noise. This “potential” is assumed to depend on two space coordinates of the plane in which the triad $\vec{T} = (R, S, I)$, describing the state of the system, evolves in time. In a simplified picture that approximates periodic orbits as being circular, one can consider polar coordinates in this plane, with their origin in the center of the periodic orbit. The angular coordinate θ describes the periodic motion of the synchronized system as it cycles around its orbit. The radial coordinate r is a measure of the intensity of synchronization, and can be taken to be proportional to the coherence z (See Eq. (3)). In Section 3.3, the noiseless dynamics for \vec{T} is argued to be approximately determined by the gradient of a potential,

while noise adds a small amount of diffusive behavior on top of that. In the absence of noise, and when starting from a mixed state (the central peak), if $\alpha < d$ the system would be attracted by, and execute a periodic motion on, the stable orbit, which is a local minimum of the potential. Because of noise, however, \vec{T} makes random excursions away from its stable orbit, until it happens to jump over the barrier and falls outwards, where synchronization attains extreme values and the dynamics becomes extinct at the outer boundary. The extinction process is, in this picture, described as noise-activated escape over a potential barrier. When $\alpha > d$ the stable orbit shrinks to zero size, rendering the endemic state $r = 0$ stable. In that case, escape occurs over the potential barrier, from a fixed point of the dynamics located at $r = 0$.

This picture, which borrows from usual approaches in the study of dynamical systems [55], provides a simple explanation for the existence of three dynamical stages, but also imposes very specific constraints on the scaling of permanence times in the different stages with system size N . Previous work regarding diffusive motion in the presence of a deterministic flow predicts that the combined time τ_0 spent in stages one and three, being these cases of motion along a flow, is only weakly affected by noise and should scale with system size also weakly, i.e as $\log N$. The permanence time in stage two, on the other hand, depends on a strongly stochastic diffusive process against a flow, that is, a noise activated escape over a potential barrier. The timescale associated with this escape process should then scale as $e^{\kappa_2 N}$. Additionally, the distribution of permanence times in stage two, according to very general arguments applying to first-passage processes, is expected to be asymptotically exponential for long times. All these predictions for the involved timescales are very well verified using the results of our numerical experiments, as discussed in Sections 3.4, 3.5, and 3.6.

Our measurements of $z_{1/2}$, the coherence at the half-time for extinction, which are shown in Fig. 3, strongly suggest that stage two has nonzero coherence z in the thermodynamic limit, only if $\alpha < d$. For larger values of α , there is some small amount of synchronization during stage two for finite systems, but it becomes smaller as N grows.

Although more work is needed to confirm the precise critical value of α in the light of previous work [33, 34, 35, 36], it is clear that, for large α , no state of sustained synchronization is expected to exist on large systems. Stage one is therefore not relevant in this case, and stage two becomes a state of non-synchronous persistent activity in which the system lingers for a long time. Then the system enters Stage three, in which explosive synchronization, followed by extinction, occurs.

If the proposed picture of a supercritical Hopf bifurcation at $\alpha = d$ is correct, then the radius of stable orbit below $\alpha = d$, shrinks to zero continuously at $\alpha = d^-$. In this case, the α -driven transition in $z_{1/2}$ that is seen in Fig. 3 is a continuous transition. The data in Fig. 3, however, could as well be compatible with a discontinuity in $z_{1/2}$ at $\alpha = d$. If this were the case, then the bifurcation at $\alpha = d$ would be a *saddle-node or fold* bifurcation (Sec. 8.4 in [55]) instead of a supercritical Hopf bifurcation, as assumed here. These two possibilities cannot be clearly distinguished on the basis of our present

data. Clearly, much more work would be needed to establish the character (continuous or discontinuous) of this α -driven transition precisely.

The fact that there is no synchronized stage two for large α , poses the question of how this modifies the picture discussed above and in Section 3.3, that describes extinction as escape over a barrier. The answer is that this picture is essentially the same in the case of large α , the only difference being that the escape process occurs now starting from a single local minimum at $z = 0$, instead as from a stable orbit with finite z . The distribution of escape times and their scaling with size, however, are expected to be the same for escape from a local minimum at large α as for escape from a stable orbit for small $\alpha \leq d$.

One of the few differences we find between one and two-dimensional systems concerns the α -dependence of $\kappa_2(\alpha, d)$ (See Fig. 11), which measures the speed of growth of $\log \tau_2$ with system size N . As seen in Fig. 11, κ_2 has a maximum near $\alpha = 2$ for one dimensional systems. This appears to be an indication of a dynamical phase transition, the origin of which we do not discuss in this work. In two dimensions, on the other hand, we find that κ_2 grows with increasing α when $\alpha > 2$ until at least $\alpha = 4$. Large values of α are not easy to simulate because of long extinction times. However, we did some simulations with $p_\alpha = 0.05$ (annealing shortens timescales) for α up to 8, without finding any sign of a nonmonotonic behavior of $\kappa_2(\alpha)$.

Acknowledgments

The authors acknowledge the use of computational resources in clusters Xiuhcoatl(CGSTIC) and Kukulcan (Dept. of Applied Physics) of CINVESTAV. EAM thanks CONACYT for support through a PhD fellowship.

- [1] Sitabhra Sinha and S. Srighar. *Patterns in excitable media: Genesis, Dynamics and Control*. CRC Press Taylor & Francis Group, 2015.
- [2] Dante R. Chialvo. Generic excitable dynamics on a two-dimensional map. *Chaos, Solitons & fractals*, 5(3/4):461–479, 1995.
- [3] Alex Roxin, Hermann Riecke, and S. A. Solla. Self-sustained activity in a small-world network of excitable neurons. *Physical Review Letters*, 92(19):198101(4), 2004.
- [4] Suhita Nadkarni and Peter Jung. Spontaneous oscillations of dressed neurons: A new mechanism for epilepsy? *Physical Review Letters*, 91(26):268101(4), 2005.
- [5] Alfonso Renart, Jaime De la Rocha, Peter Bartho1, Liad Hollender, Néstor Parga, Alex Reyes, and Kenneth D. Harris. The asynchronous state in cortical circuits. *Science*, 327:587–590, 2010.
- [6] Alexander S. Ecker, Philips Berens, Georgios A. Keliris, Matthias Bethge, Nikos K. Logothetis, and Andreas S. Tolias. Decorrelated neuronal firing in cortical microcircuits. *Science*, 327:584–587, 2010.
- [7] Néstor Parga. Towards a self-consistent description of irregular and asynchronous cortical activity. *Journal of Statistical Mechanics: Theory and Experiment*, 2013(03):P03010, 2013.
- [8] Marcelo Kuperman and Guillermo Abramson. Small world effects in an epidemiological model. *Physical Review Letters*, 86(13):2909(4), 2001.
- [9] Steven H. Strogatz. *Sync: the emerging science of spontaneous order*. Hyperion, 1st edition, 2003.
- [10] Onno A. van Herwaarden and Johan Grasman. Stochastic epidemics: major outbreaks and the duration of the endemic period. *Journal of Mathematical Biology*, 33:581–601, 1995.
- [11] Quan-Xin Liu, Rong-Hua Wang, and Zhen Jin. Persistence, extinction and spatio-temporal

- synchronization of sirs spatial models. *Journal of Statistical Mechanics: Theory and Experiment*, 2009(07):P07007, 2009.
- [12] Seung Ki Baek. Oscillatory behaviors of an epidemiological model on small-world networks. *Journal of the Korean Physical Society*, 50(1):320–326, 2007.
- [13] Paolo Bajardi, Chiara Poletto, José J. Ramasco, Michele Tizzoni, Vittoria Colizza, and Alessandro Vespignani. Human mobility networks, travel restrictions, and the global spread of 2009 h1n1 pandemic. *Plos One*, 6:e16591(8), 2011.
- [14] Cécile Viboud, Ottar N. Bjørnstad, David L. Smith, Lone Simonsen, Mark A. Miller, and Bryan T. Grenfell. Synchrony, waves, and spatial hierarchies in the spread of influenza. *Science*, 312(5772):447–451, 2006.
- [15] Duygu Balcan, Vittoria Colizza, Bruno Gonçalves, Hao Hu, José J. Ramasco, and Alessandro Vespignani. Multiscale mobility networks and the spatial spreading of infectious diseases. *PNAS*, 106(51):21484–21489, 2009.
- [16] Duygu Balcan, Bruno Gonçalves, Hao Hu, José J. Ramasco, Vittoria Colizza, and Alessandro Vespignani. Modeling the spatial spread of infectious diseases: The global epidemic and mobility computational model. *Journal of Computational Science*, 1:132–145, 2010.
- [17] Stefano Merler and Marco Ajelli. The role of population heterogeneity and human mobility in the spread of pandemic influenza. *Proc. R. Soc. B*, 277:557–565, 2010.
- [18] Pascal Fries. A mechanism for cognitive dynamics: neuronal communication through neuronal coherence. *Trends in Cognitive Sciences*, 9:474–480, 2005.
- [19] Marie-Therese Horstmann Dieter Krug Alexander Rothkegel Matthus Staniek Tobias Wagner Klaus Lehnertz, Stephan Bialonski. Synchronization phenomena in human epileptic brain networks. *Journal of Neuroscience Methods*, 183:42–48, 2009.
- [20] J. C. Stam. Nonlinear dynamical analysis of eeg and meg: Review of an emerging field. *Clinical Neurophysiology*, 116, 2005.
- [21] Ying-Cheng Lai, Mark G. Frei, Ivan Osorio, and Liang Huang. Characterization of synchrony with applications to epileptic brain signals. *Phys. Rev. Lett.*, 98:108102, 2007.
- [22] P. Tass, M. G. Rosenblum, J. Weule, J. Kurths, A. Pikovsky, J. Volkmann, A. Schnitzler, and H.-J. Freund. Detection of $n : m$ phase locking from noisy data: Application to magnetoencephalography. *Phys. Rev. Lett.*, 81:3291 – 3294, 1998.
- [23] Johan Grasman and Onno A. van Herwaarden. *Asymptotic Methods for the Fokker-Planck Equation and the Exit Problem in Applications*. Springer-Verlag Berlin Heidelberg, first edition, 1999.
- [24] Zeev Schuss. *Theory and applications of stochastic differential equations*. John Wiley & Sons, first edition, 1980.
- [25] H. Roosen. An asymptotic solution to a two-dimensional exit problema arising in population dynamics. *SIAM Journal of Applied Mathematics*, 49(6):1793–1810, 1989.
- [26] Tobias Reichenbach, Mauro Mobilia, and Erwin Frey. Coexistence versus extinction in the stochastic cyclic lotka-volterra model. *Physical Review E*, 74(5):051907(11), 2006.
- [27] Jonas Cremer, Tobias Reichenbach, and Erwin Frey. The edge of neutral evolution in social dilemmas. *New Journal of Physics*, 11:093029(15), 2009.
- [28] Alexander Dobrinevski and Erwin Frey. Extinction in neutrally stable stochastic lotka-volterra models. *Physical Review E*, 85(5):051903(12), 2012.
- [29] Ingemar Nåsell. On the time to extinction in recurrent epidemics. *J.R. Statist. Soc. B*, 61:309–330, 1999.
- [30] Miguel González, Rodrigo Martínez, and Maroussia Slavtchova-Bojkova. *Workshop on branching processes and their applications - Chapter 17, pages 241–256*. Springer-Verlag Berlin Heidelberg, 2010.
- [31] S. Boccaletti, V. Latora, Y. Moreno, M. Chavez, and D.-U. Hwang. Complex networks: Structure and dynamics. *Physics Reports*, 424(4):175 – 308, 2006.
- [32] Alex Arenas, Albert Díaz-Guilera, Kurths Jürgen, Yamir Moreno, and Chansong Zhou.

- Synchronization in complex networks. *Physics Reports*, (469):93–153, 2008.
- [33] Hiroaki Daido. Lower critical dimension for populations of oscillators with randomly distributed frequencies: A renormalization-group analysis. *Phys. Rev. Lett.*, 61:231–234, 1988.
- [34] Hietsugu Sakaguchi, Shigeru Shinimoto, and Yoshiki Kuramoto. Local and global self-entrainments in oscillator lattices. *Progress of Theoretical Physics*, 77(5):1005–1010, 1987.
- [35] H. Hong, Hyunggyu Park, and M. Y. Choi. Collective synchronization in spatially extended systems of coupled oscillators with random frequencies. *Phys. Rev. E*, 72:036217, 2005.
- [36] Debanjan Chowdhury and M.C. Cross. Synchronization of oscillators with long-range power law interactions. *Physical Review E*, 82(1):011605(12), 2010.
- [37] T. Binzegger, R.J. Douglas, and K.A.C Martin. A quantitative map of the circuit of cat primary visual cortex. *J. Neurosci.*, (24):84418453, 2004.
- [38] F.E. Lebeau R. Maex H. Markram G. Silberberg, S. Grillner. Synaptic pathways in neural microcircuits. *Trends Neurosci.*, (28):541551, 2005.
- [39] Y. Wang A. Gupta G. Silberberg C. Wu H. Markram, M. Toledo-Rodriguez. Interneurons of the neocortical inhibitory system. *Nature Rev. Neurosci.*, (5):793–807, 2004.
- [40] Thomas K. Berger Rodrigo Perin and Henry Markram. A synaptic organizing principle for cortical neuronal groups. *PNAS*, 108(13):54195424, 2011.
- [41] A. Ylinen G. Buzsaki A. Sik, M. Penttonen. Hippocampal cal interneurons: An in vivo intracellular labeling study. *J. Neurosci.*, (15):66516665, 1995.
- [42] A. Schüz V. Braitenberg. *Cortex: Statistics and Geometry of Neuronal Connectivity*. Springer-Verlag, Heidelberg, Germany, 2nd edition, 1998.
- [43] M. Penttonen G. Buzsaki A. Sik, A. Ylinen. Inhibitory cal-ca3-hilar region feedback in the hippocampus. *Science*, 265:1722–1724, 1994.
- [44] J. Karbowski. Optimal wiring principle and plateaus in the degree of separation of cortical neurons. *PRL*, 86(16):3674, 2001.
- [45] Claus C. Hilgetag Marcus Kaiser. A simple rule for axon outgrowth and synaptic competition generates realistic connection lengths and filling fractions. *Cerebral Cortex*, 19:3001, 2009.
- [46] Zhang J. Chen Yong He and Alan C. Evans McConnell. Small-world anatomical networks in the human brain revealed by cortical thickness from mri. *Cerebral Cortex*, 17:2407–2419, 2007.
- [47] Victor M. Eguíluz, Dante R. Chialvo, Guillermo A. Cecchi, Marwan Baliki, and A. Vania Apkarian. Scale-free brain functional networks. *Phys. Rev. Lett.*, 94:018102, Jan 2005.
- [48] L. Hufnagel D. Brockmann and T. Geisel. The scaling laws of human travel. *Nature*, 439:462–465, 2006.
- [49] Cristian F. Moukarzel. Effective dimensions in networks with long-range connections. *Physica A: Statistical Mechanics and its Applications*, 356(1):157 – 161, 2005. Nonequilibrium Statistical Mechanics and Nonlinear Physics (MEDYFINOL’04).
- [50] Herbert W. Hethcote, Harlan W. Stech, and P. Van Den Driessche. Nonlinear oscillations in epidemic models. *SIAM Journal of Applied Mathematics*, 40(1):1–9, 1981.
- [51] S. Gonçalves, G. Abramson, and M.F.C. Gomes. Oscillations in sirs model with distributed delays. *The European Physical Journal B*, 83(1):363–371, 2011.
- [52] Yoshiki Kuramoto. *Chemical Oscillations, Waves, and Turbulence*. Springer, 1st edition, 1984.
- [53] Steven H. Strogatz. From kuramoto to crawford: exploring the onset of synchronization in populations of coupled oscillators. *Physica D*, 143:1–20, 2000.
- [54] P. Erdős and A. Rényi. On the evolution of random graphs. *Mathematikai Katutó Intézet Közleményei*, 5:17–61, 1960.
- [55] Steven H. Strogatz. *Nonlinear Dynamics and Chaos*. Westview Press, 11 Cambridge Center, Cambridge, MA, 1st edition, 1994.
- [56] Sydney Redner. *A Guide to First-Passage Processes*. Cambridge University Press, 1st edition, 2001.